

Fragility curves and loss functions for RC structural components with smooth rebars

Donatello Cardone*

School of Engineering, University of Basilicata, Viale Ateneo Lucano 10, 85100 Potenza, Italy

(Received July 7, 2015, Revised February 5, 2016, Accepted February 27, 2016)

Abstract. Fragility and loss functions are developed to predict damage and economic losses due to earthquake loading in Reinforced Concrete (RC) structural components with smooth rebars. The attention is focused on external/internal beam-column joints and ductile/brittle weak columns, designed for gravity loads only, using low-strength concrete and plain steel reinforcing bars. First, a number of damage states are proposed and linked deterministically with commonly employed methods of repair and related activities. Results from previous experimental studies are used to develop empirical relationships between damage states and engineering demand parameters, such as interstory and column drift ratios. Probability distributions are fit to the empirical data and the associated statistical parameters are evaluated using statistical methods. Repair costs for damaged RC components are then estimated based on detailed quantity survey of a number of pre-70 RC buildings, using Italian costing manuals. Finally, loss functions are derived to predict the level of monetary losses to individual RC components as a function of the experienced response demand.

Keywords: fragility functions; damage states; RC frame buildings; beam-column joints; weak columns; smooth reinforcing bars; repair methods; repair costs; loss functions; FEMA P-58

1. Introduction

Past earthquakes have shown that seismic events may incur large economic losses due to damage in buildings and other structures, which in many cases were unexpected to owners and other stakeholders. One of the most promising tools that can be used to estimate damage, hence losses, resulting from an earthquake is the so-called Performance-Based Earthquake Engineering (PBEE) (Bozorgnia and Bertero 2004). PBEE is emerging as the next-generation design and evaluation framework under which new and existing structures will be analyzed for seismic adequacy. PBEE implies design, evaluation, and construction of engineered facilities whose performance, under service and extreme loads, responds to the diverse needs and objectives of owners and other stakeholders. Recently, FEMA contracted with ATC the development of a seismic performance assessment methodology. The work was completed in 2012 with the publication of two volumes collectively referred to as FEMA P-58 (ATC 2012a, b). For practical

*Corresponding author, Professor, E-mail: donatello.cardone@unibas.it

implementation of the methodology, work included the development of an electronic tool, referred to as the Performance Assessment Calculation Tool (PACT). The PBEE approach implemented in FEMA-P-58 appears to be very attractive and promising, because it utilizes performance measures that can be understood by decision makers. In FEMA-P-58, indeed, future seismic performance of buildings is expressed in terms of repair costs, fatalities, and repair duration (dollars, deaths, and downtime).

In the probabilistic framework proposed in FEMA-P-58, estimation of economic losses is performed in three steps. In the first step, a probabilistic description of the seismic demand to the structure is obtained from results of response-time history analyses at increasing levels of ground motion intensity. In the second step, damage to individual structural and nonstructural components is estimated as a function of the engineering demand parameters (e.g., peak interstory drifts, etc.) computed in the first step. This requires fragility functions for various damage states for each component in the facility. In the third step, economic losses to individual components are estimated as a function of the level of damage sustained by each component. This approach requires loss functions for various damage states for each component in the facility.

At the moment, specific tools (i.e., fragility and loss functions) for the PBEE analysis of older RC frame buildings are missing. The buildings under consideration include those realized before '70s (i.e., before the introduction of modern seismically oriented codes), which were designed for gravity loads only, using low-strength concrete and plain steel reinforcing bars, and that feature masonry infills as non-structural exterior walls and internal partitions. Such buildings represent a large part of the building stock of Italy* and many other European countries. The scope of this paper is to partly fill this gap, developing fragility and loss functions for the typical structural components of pre-70 RC frame buildings, which can be implemented in PACT for PBEE analysis. Similar studies concerning masonry infills and partitions are presented in (Cardone and Perrone 2015).

2. Fragility Groups

The main objective of this study is to summarize results from previous experimental studies on laboratory RC specimens with design details representative of pre-70 RC frame buildings, in order to develop fragility functions that permit the estimation of damage in critical components of pre-70 RC frame buildings as a function of attained peak interstory drift. The year 1970 is taken as a reference for the appearance of modern seismic codes, aiming at a ductile design of the structural components. In the US, for instance, seismic design provisions were introduced into the 1967 Uniform Building Code (ICBO 1967) and in the 1971 ACI-318 code (ACI 1971). Similarly, in Italy, the first seismic design provisions were introduced with the issue of the Law n. 64 (GU 1974) in February 1974.

Reinforced concrete (RC) structures built before '70s (i.e., before the introduction of modern seismically oriented codes) were usually designed for gravity loads only, using low-strength concrete and plain steel reinforcing bars. As a consequence of the absence of any capacity design criterion and poor reinforcement details, a significant lack of ductility - at both local and global level - is expected for these structures, resulting in inadequate structural performance even under

*More than 60% of the buildings in Italy, some 7 million, was built before 1972. Large part of this building stock consists of RC frame buildings (Source: ANCE processing of ISTAT data)

moderate seismic excitations.

Past experimental investigations (Calvi *et al.* 2002, El-Attar *et al.* 1997, Bracci *et al.* 1995) and damage observed following recent earthquakes indicate that damage/collapse mechanisms of pre-70 RC frame buildings can be related to one or more of the following aspects: (i) Deficiencies in detailing of beam-column joints, which often lead to brittle failure of connection; Different damage/failure modes are expected to occur depending on the typology (exterior or interior joint) and adopted structural details (e.g., total lack of transverse reinforcement, alternative anchorage solutions, etc.); (ii) Effects of bar slippage (fixed-end rotation mechanism), which are particularly relevant in presence of plain reinforcing bars due to the poor concrete-steel bond properties associated with this type of steel; (iii) Insufficient anchorage and lap lengths and (iv) Strong interaction between masonry infills and RC frame.

All that considered, five different Fragility Groups (FGs) of structural components have been identified for typical pre-70 RC frame buildings, i.e., (1) External beam-column joints, with Weak Joints and beam flexural response (EWJs), (2) Internal beam-column joints, with Weak Beams and column flexural response (IWBs), (3) Internal beam-column joints, with Weak Columns and beam flexural response (IWCs), (4) Ductile Weak Columns (DWCs), with strong joints and end-hook rebars (e.g., base columns), liable to flexural failure and (5) Brittle Weak Columns (BWCs), liable to shear failure before developing plastic hinges (e.g., short columns around staircase). The expected behavior under cyclic loading of the aforesaid five FGs is first examined, to identify typical crack/damage patterns to be considered for repair interventions.

It is widely recognized that exterior beam-column joints play a fundamental role in the seismic performance of older moment resisting RC frames, due to lack of a reliable joint shear transfer mechanism (Pampanin *et al.* 2002, Braga *et al.* 2009). This poor behavior is mainly due to: inadequate reinforcement detailing (lack of transverse reinforcement in the joint region), poor bond properties of the reinforcement (use of plain round bars) and deficiencies in the anchorage details (bars with end-hooks). External beam-column joints, with Weak Joints and beam flexural response (EWJs) exhibit a brittle hybrid failure mechanism due to joint shear damage combined with slippage of longitudinal beam bars within the joint region, combined with concentrated compressive force at the end-hook anchorage. As a result, a concrete “wedge” forms, which tend to spall off, leading to brittle local failure and loss of bearing-load capacity.

Interior beam-column joints show a completely different behavior, with significant resources of plastic deformation, even without specific ductile structural details (Fernandes *et al.* 2013). This is due to the concentration of flexural cracks at the beam-joint (IWBs) or column-joint (IWCs) interfaces, which act as a structural fuse for the joint panel zone, which does not suffer any damage. In both cases, a fundamental role is played by the poor bond between plain longitudinal reinforcing bars and surrounding concrete, which leads to marked pinching effects and cyclic deterioration. From this point of view, the anchorage solutions with lapped splices and end hooks show a better behavior compared to continuous reinforcement (Fernandes *et al.* 2013).

Dimensional proportioning of columns and beams in old buildings was usually carried out in a way that beams have much more flexural stiffness and strength than columns. Consequently, failure mode of old RC buildings is often due to soft story mechanisms (Hakuto *et al.* 2000). In many cases, the soft storey is the first storey due to the lack (or lower effectiveness) of masonry infills. Deformation mechanism of concrete columns with smooth bars is much different from those with deformed bars (Arani *et al.* 2013). The differences are mostly due to the development of a fixed-end rotation collapse mechanism. Once again, the bond properties and reinforcement detailing play a relevant role in the development of the rotation capacity of plastic hinges of base

columns with plain rebars. In particular, rotational deformations develop through the opening of large flexural cracks, localized at the interface between column and foundation block, in case of overlapped longitudinal bars, while they spread over the column length when continuous longitudinal bars are used.

Past earthquakes, moreover, pointed out that older substandard RC structural elements are often more liable to fail in shear than in flexure, due to the low amount of stirrups. This is the case of the short columns framed by the knee beams of the stairs in older RC buildings. Recent experimental tests (Henkhaus 2010) confirmed that short columns experience premature inclined cracks followed by the loss of lateral-force capacity (shear failure). Shear failure may lead to axial column failure. Based on observations from tests performed by Lynn (2001) and Sezen (2002), the ability of columns to sustain axial load after shear failure appears to be closely related to the portion of the load carried by the longitudinal reinforcement. When the axial load reaches a critical value, steel rebars fail, resulting in the axial failure of the column.

The aforesaid considerations emphasize the peculiarity of each FG and the need of defining specific fragility functions for each of them, also taking into account possible further differentiations related to different structural details.

3. Definition of damage states

For each FG, a number of Damage States (DSs) has been defined to characterize damage progression in the RC components under scrutiny. Damage states are defined by the extent and severity of concrete cracking, concrete crushing, yielding of reinforcing steel, buckling of reinforcing steel, etc., supported or complemented by other macroscopic damage indicators, such as the attainment of the peak force or given ratios of strength reduction.

In this study, in particular, three discrete DSs have been defined for each FG, based on specific repair actions that would have to be taken as a result of the observed damage. This approach facilitates the estimation of economic losses and other types of consequences (e.g., repair time, etc.) resulting from the occurrence of damage.

The first DS is basically associated with light cracking of concrete. Generally speaking, at DS1, damage results in slight opening of well-localized concrete cracks and first yielding of longitudinal bars. Concrete repair (typically with epoxy injections) may be required to restore component stiffness and strength as well as to ensure that earthquake damage does not make the component vulnerable to water infiltration, corrosion, fire damage, etc. Expected crack patterns for each FG are defined as follows:

- EWJs (see Fig. 1(a)): light cracking (residual crack width $<1-1.5$ mm) at beam-joint (or less likely column-joint) interfaces, and possible first inclined joint cracks. A second crack on beam is also expected at a distance equal to half beam height, due to yielding of beam rebars.

- IWBs (see Fig. 2(a)): cracking onset at beam-joint interfaces (residual crack width $<1-1.5$ mm), due to the combined effect of slippage and yielding of steel rebars. Flexural cracks in beams develop both at top and bottom edges and may extend over the entire height of the beam under cyclic loading. Further cracks may develop up to a distance of the order of half the beam height. Possible minor cracks in the columns (at the column-joint interface and at a distance equal to half the column depth) may be observed.

- IWCs: The crack pattern is similar to that described above for IWB, with the only difference that it involves columns instead of beams.

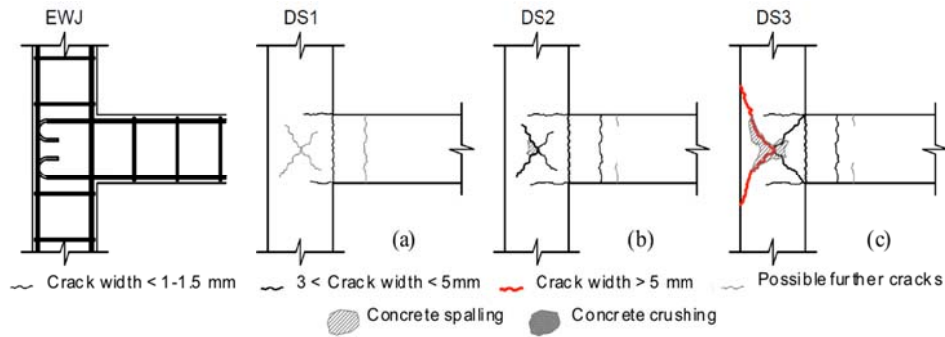


Fig. 1 Damage states of external RC beam-column joints with plain rebars with end-hooks

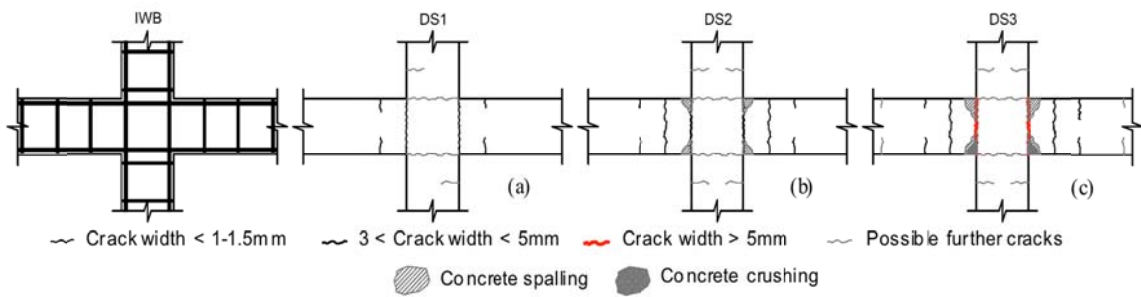


Fig. 2 Damage states of internal beam-column joints with weak beams and column flexural response

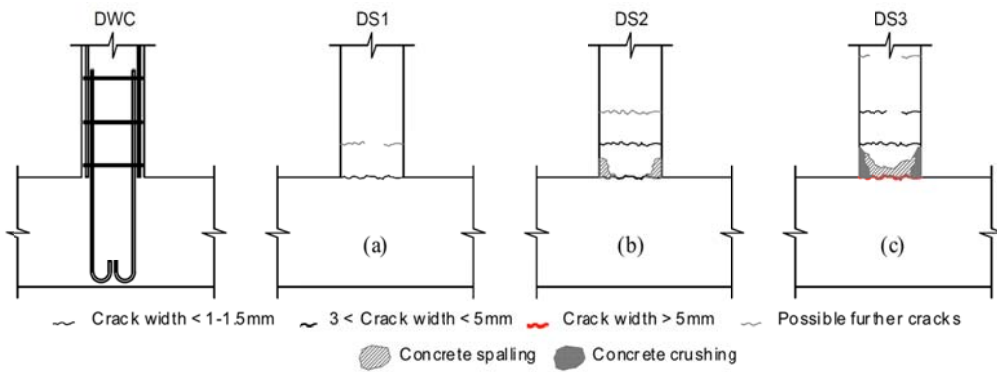


Fig. 3 Damage states of ductile weak columns featuring strong joint and end-hook rebars

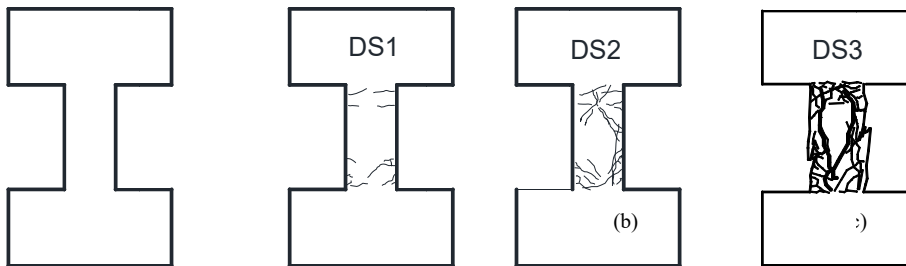


Fig. 4 Damage states of brittle weak columns (e.g., short columns around staircase)

- DWCs (see Fig. 3(a)): yielding of column rebars, light opening (<1-1.5 mm) of concrete cracks at the base of the column. In presence of lap-spliced bars, further cracks may develop up to a distance of the order of half the column depth.

- BWCs (see Fig. 4(a)): development of light horizontal cracks in the upper and lower thirds of the column.

The second DS is basically associated with onset of concrete spalling. Generally speaking, at DS2, the concrete cracks developed at DS1 tend to widen. Minor new cracks may form in beams, columns or joints. In many cases, damage includes spalling of small portions of cover concrete that expose beam or column transverse reinforcement. In that case, replacement of spalled concrete is required to avoid that exposed rebars are vulnerable to corrosion, fire damage, etc., as well as to restore component lateral strength and stiffness. Calculation of loss associated with structural repair for DS2 requires calculation of the length of cracks to be injected as well as the surface of concrete area to be patched. The following damage patterns have been assumed in this study for the DS2 of the RC components under consideration:

- EWJs (see Fig. 1(b)): existing cracks, at beam-joint interface, widen (3 mm < residual crack width < 5 mm). Further cracks at a distance of the order of 3/4 the beam height may develop. Spalling of cover concrete is expected in the joint, involving an area of the order of 10% the area of the joint panel.

- IWBs (see Fig. 2(b)): existing cracks at beam-joint interfaces widen (3 mm < residual crack width < 5 mm). Further cracks at a distance of the order of the beam height may develop. Minor cracks at the column-joint interfaces may occur. Spalling of beam cover concrete is expected, near the joint, both at top and bottom beam edge, for a length of the order of 10% the beam depth.

- IWCs: The damage pattern is similar to that described above for IWB, with the only difference that it involves columns instead of beams.

- DWCs (see Fig. 3(b)): the existing crack at the base of the column widen (3 mm < residual crack width < 5 mm), according to the fixed-end rotation mechanism. Additional column cracks are possible up to a distance of the order of the column height. Spalling of cover concrete is expected at the base of the column, near the section corners, for a length of the order of 10% the column depth.

- BWCs (see Fig. 4(b)): development of extensive double diagonal cracks along the entire height of the column, corresponding to the shear failure (attainment of the lateral strength) of the column.

It is worth noting that the crack width limits mentioned in the description of the crack patterns associated with DS1 and DS2 have been defined summarizing experimental findings from a number of experimental studies (e.g., Braga *et al.* 2009 for EWJ, Verderame *et al.* 2008 for DWC, Fernandes *et al.* 2013 for IWB/IWC) in which local deformation and crack evolution were monitored during the tests using LVDTs.

The third DS is basically associated with onset of concrete crushing. Generally speaking, at DS3, spalling of cover concrete is diffused and exposes both transverse and longitudinal reinforcement. Concrete damage may involve crushing of concrete core. It may be necessary to remove and recast concrete portions of some RC members. Bar buckling may also occur. Calculation of loss associated with structural repair for DS3 requires evaluation of the extension of concrete cracking to be epoxy injected, as well as evaluation of the volume of concrete to be removed and recast, and eventually the number of bars to be replaced. In the first approximation, it has been assumed that the concrete cracks to be injected were the same as DS2. In addition, the following damage pattern has been assumed:

- EWJs (see Fig. 1(c)): Damage tends to concentrate in the joint, through the appearance of interconnected cracks, progressive spalling of cover concrete and activation of a concrete wedge expulsion collapse mechanism. Spalling of concrete is expected to involve an area of the order of 30% the joint panel. Buckling of column longitudinal rebars may also occur.

- IWBs (see Fig. 2(c)): Extensive spalling of cover concrete at the beam intrados is expected, over an area involving the whole depth of the beam, for a length of the order of 20% the beam depth. Possible crushing of concrete at beam-joint interfaces. Further minor cracks may develop in the beams at a distance from the joint up to twice the beam height.

- IWCs: The damage pattern is similar to that described above for IWB, with the only difference that it involves columns instead of beams. In addition, possible buckling of longitudinal rebars is expected.

- DWCs (see Fig. 3(c)): Loss of strength due to extensive spalling of cover concrete is expected, along the whole section perimeter, for a length equal to the column depth. Crushing of concrete core in the section corners is likely to occur. Concrete cracking may extend further, involving a column length (from the base of the column) twice the column height. Buckling of longitudinal rebars may also occur.

- BWCs (see Fig. 4(c)): Opening of large cracks. Buckling of steel rebars. Attainment of residual lateral strength. Possible significant loss of gravity load capacity, due to incipient failure of distorted longitudinal reinforcement.

The fourth DS can be associated with the (incipient) collapse of the RC component. In particular, the collapse of EWJs can be ascribed to loss of vertical carrying capacity due to the development of the concrete wedge expulsion collapse mechanism. The collapse of IWBs, on the other hand, can be ascribed to either fracture or pull-out of steel rebars. Buckling of longitudinal rebars is expected to trigger collapse for IWCs. Finally, the collapse of DWCs and BWCs can be ascribed to loss of vertical carrying capacity due to the significant reduction of the resistant concrete section, as a consequence of concrete crushing and spalling, buckling or fracture of longitudinal rebars, P-Delta effects. Economic losses associated with DS4 are not considered because structural repair for DS4 is very difficult to be realized in practice and costs are very high.

4. Experimental results used in this study

Two criteria have been adopted to select experimental data sets for this study. First, only laboratory tests on specimens with design details representative of pre-70 RC buildings (use of plain rebars, lack of stirrups in the joint, etc.) have been considered. Second, only laboratory test specimens with the same basic configuration and load pattern have been selected. In particular, two types of laboratory specimens have considered: (i) sub-assemblages from two-dimensional building frames, comprising the joint, the beam(s) framing into the joint and extending to mid-span, and the columns framing into the joint and extending to mid-height, (ii) cantilever schemes consisting in half-height column specimens restrained by a rigid foundation block.

It is worth noting that test specimens represent bare frames, and the impact of masonry infills (as well as concrete floor slab) on the sub-assemblage response and damage progression is not considered, in accordance with current practice (e.g., see Annex A of FEMA-P-58). Obviously, in case of a real structure, masonry infills (and floor slabs) also are present within frames and they do affect its seismic response, especially at low-to-moderate seismic intensities. However, this is implicitly taken into account with the introduction of an additional contribution to fragility

dispersion, as explained in paragraph 5.4.

In the experimental tests, lateral loading was applied as a shear force lumped at the top of the column and reacted by shear forces at the base of the column and beam end(s). The lateral force was applied pseudostatically through a prescribed cyclic displacement history, consisting of one or more cycles at increasing displacement amplitudes. A constant axial load was applied at the top of the column to simulate gravity load.

In this study, Interstory Drift Ratio (IDR) or Column Drift Ratio (CDR) have been chosen as engineering demand parameters, to describe the evolution of earthquake damage in RC members.

Generally speaking, in many cases, there was not enough information to establish the drift ratios at which all three damage states take place. This occurs either because the damage state did not occur or because the research report does not document in detail information to properly establish the level of drift at which the damage state was observed. The later situation was particularly common for the first two damage states (light cracking and severe cracking), primarily because experimental test are typically concerned with peak strength and ultimate displacement capacity rather than damage control. As a matter of fact, only a few investigations have reported detailed information about cracking patterns and crack widths at various levels of lateral deformation.

Previous studies (Pan and Moehle 1988) suggest that cracking levels where concrete repair with epoxy injection is needed, typically occurs when top steel reinforcement is at yield or close to yielding. Therefore, in order to gather more data points associated with the first damage state, it was assumed that when no specific information on crack patterns and crack widths was available, DS1 occurs at peak interstorey drifts at which top steel reinforcement was reported to yield or at peak interstorey/column drifts at which first significant residual drift in the hysteresis loop was observed after unloading.

Similar problems were faced when trying to determine the interstorey/column drifts associated with the second damage state. As a consequence, in order to expand the number of data points associated with the second damage state, reference to either the interstorey/column drift at which clearly visible concrete spalling was reported by the investigators or, alternatively, the interstorey/column drift at which the peak strength in the hysteresis loop was attained, has been made. Finally, for DS3, reference to either the interstorey/column drift at which extensive concrete spalling and first significant signs of concrete crushing (or steel buckling) was reported by the investigators or, alternatively, the interstorey/column drift at which a strength loss of 20% in the hysteresis loop was observed, has been made. It should be noted that a similar approach was followed also in previous studies (e.g., Pagni and Lowes 2006, Aslani and Miranda 2005, etc.). Moreover, the assumptions made in this study are empirically substantiated by the examined hysteresis loops. In other words, when specific information on the damage pattern was available, concrete spalling was observed to begin around the interstorey/column drift at which the peak strength was attained; Similarly, concrete crushing was reported to occur around the interstorey/column drift at which a strength loss of 20% was observed, etc.

4.1 External beam-column joints

Information about the material properties and characteristics of all external beam-column joint specimens considered in this study is summarized in Table 1, which includes results from seven different experimental investigations on seventeen laboratory specimens. Two types of specimens have to be distinguished (see column labeled with “Long. reinf. details” in Table 1), i.e., specimens in which the longitudinal bars were anchored in the joint with end-hooks and specimens

in which the longitudinal bars were bent in the joint.

In Table 1, columns with header “section” provide the section width and height dimensions of beams and columns, ρ_{long} is the longitudinal reinforcement ratio of beams and columns (computed as A_{sl}/bh , where A_{sl} is the area of the longitudinal reinforcement, b is the section width, and h is the section height), ρ_{transv} is the transverse reinforcement ratio of beams and columns (computed as A_{st}/bs , where A_{st} is the transverse reinforcement area in the direction of loading and s is the tie spacing), f_{ym} and f_{tm} are the average yield strength and ultimate strength of steel, respectively, f_{cm} is the average compressive strength of concrete, and P is the applied axial load. The reference paper/report for each experimental investigation is reported in the second column of Table 1.

Table 5 presents the interstory drifts associated with DS1 (light concrete cracking), DS2 (concrete spalling) and DS3 (concrete crushing) of external beam-column joints. As can be seen, based on the available experimental data, the first damage state in external beam-column joints occurs at interstory drift ranging from 0.4% to 1%. Interstory drifts associated with the attainment of DS2(DS3) exhibit a larger dispersion, being reported to occur for interstory drifts as small as 0.9(1.75)% or as large as 2.39(4)%. In presence of longitudinal rebars anchored in the joint with end-hooks, the interstory drift associated with DS1 results, on average, higher than for specimens with rebars bent in the joint. The contrary holds for interstory drifts associated with DS2 and DS3.

4.2 Internal beam-column joints

Information about the material properties and characteristics of all internal beam-column joint

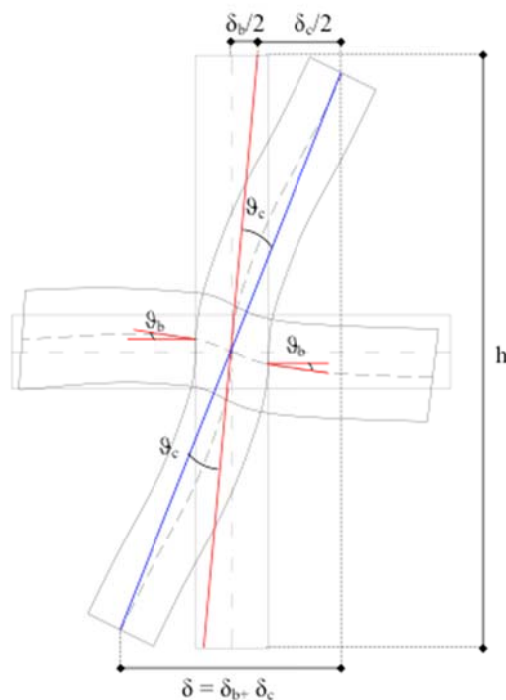


Fig. 5 Frame sub-assembly deformation due to bending of column and beam

specimens considered in this study is summarized in Table 2, which includes results from four different experimental investigations for a total of ten laboratory specimens. All the specimens feature continuous reinforcement in the joint (no specimens with lapped spliced bars with hooked-end anchorage outside the joint region). Table 5 summarizes the interstory drifts associated with DS1, DS2 and DS3 of internal beam-column joints. As can be seen, based on the available experimental data, the first damage state in internal beam-column joints occurs at interstory drift ranging from 0.46% to 0.875%. For two specimens it was not possible to identify the interstory drift associated with DS1. Interstory drifts associated with DS2 range between 1.5% and 2.25% of the story height. Finally, the interstory drifts corresponding to the attainment of DS3 is reported to occur for interstory drifts ranging from 2.1% to 3.3%.

4.3 Ductile and brittle weak columns

Information about the material properties and characteristics of ductile column specimens (experiencing flexural failure) considered in this study is summarized in Table 3, which includes results from six different experimental investigations on twenty four laboratory specimens. Two types of specimens can be distinguished (see column labeled with “Long. reinf. details” in Table 3), i.e., specimens with continuous longitudinal reinforcement bars and specimens with overlapped longitudinal reinforcement bars.

For BWCs, the main characteristics of the specimens considered in this study are summarized in Table 4, which includes results from five different experimental investigations on eighteen laboratory specimens, including short ($h_c/d_c < 3$) and slender columns ($h_c/d_c \geq 3$). All specimens, tested in single or double curvature, were designed to experience shear failure before developing plastic hinges. During the tests, a constant axial compressive load was applied to columns while being subjected to lateral deformations with increasing amplitude, till loss of axial load capacity.

Table 6 summarizes the column drift ratios associated with DS1, DS2 and DS3 of ductile and brittle columns. It should be noted that the column drift ratio (i.e., the chord rotation in the column) differs from the interstory drift ratio, depending on the relative stiffness of the beams with respect to the columns (see Fig. 5). Strictly speaking, therefore, it is not correct to enter the fragility curves proposed in this study with the interstory drift ratios derived from structural analysis, since not all of this drift demand generates deformation in the columns, part of it being associated with deformation of beams (see Fig. 5).

Looking at Table 5, negligible differences (on average less than 10%), in terms of column drift ratios associated with DS1 and DS2, are observed between columns with continuous and overlapped rebars. For RC columns with overlapped rebars, the column drift ratios associated with DS3 result higher (on average by 25%) than in presence of continuous rebars.

5. Evaluation of fragility functions

As shown in the previous tables, the drift ratios at which each damage state is reported to occur show important variations from one specimen to another. In order to estimate how likely it is that a given damage state will occur in a structure undergoing a specific level of drift, it is necessary to take into account this specimen-to-specimen variability. This uncertainty can be explicitly taken into account by developing drift-based fragility functions.

Table 1 Properties of RC exterior beam-column joint specimens considered in this study

Specimen ID	Reference	Label	f_{ym} (MPaa)	f_{tm} (MPa)	f_{cm} (MPa)	Beam section (cm*cm)	$\rho_{long,b}$ (%)	$\rho_{transv,b}$ (%)	Column section (cm*cm)	$\rho_{long,c}$ (%)	$\rho_{transv,c}$ (%)	L_b/L_c	$\rho_{transv,j}$ (%)	P (KN)	Long. reinf. details	Loading protocol
1	Braga <i>et al.</i> (2009)	T23-1	350	460	14.5	20*33	0.49 ⁽⁺⁾ 0.32 ⁽⁻⁾	0.12	20*20	1.13	0.12	1.4	0.0	120	Anchored with end-hook in the joint	Cyclic
2	Pampanin <i>et al.</i> (2003)	T1	345	458	23.9	20*33	0.49 ⁽⁺⁾ 0.49 ⁽⁻⁾	0.11	20*20	0.75	0.10	1.5	0.0	100		
3		T1	345	458	23.9	20*33	0.49 ⁽⁺⁾ 0.49 ⁽⁻⁾	0.11	20*20	0.75	0.10	1.5	0.0	100		
4	Bedirhanoglu <i>et al.</i> (2010)	JO1	333	470	8.3	25*50	0.64 ⁽⁺⁾ 0.64 ⁽⁻⁾	0.4	25*50	1.28	0.26	1.12	0.0	130	Bent in the joint	Cyclic
5		JO2	333	470	8.3	25*50	0.64 ⁽⁺⁾ 0.64 ⁽⁻⁾	0.4	25*50	1.28	0.26	1.12	0.04	-		
6		JO3	333	470	8.3	25*50	0.64 ⁽⁺⁾ 0.64 ⁽⁻⁾	0.4	25*50	1.28	0.26	1.12	0.16	-		
7		JO4	333	470	8.3	25*50	0.64 ⁽⁺⁾ 0.64 ⁽⁻⁾	0.4	25*50	1.28	0.26	1.12	0.0	520		
8		JO5	333	470	8.3	25*50	0.64 ⁽⁺⁾ 0.64 ⁽⁻⁾	0.4	25*50	1.28	0.26	1.12	0.0	130		
9		JO6	333	470	8.3	25*50	0.64 ⁽⁺⁾ 0.64 ⁽⁻⁾	0.4	25*50	1.28	0.26	1.12	0.0	-		
10		JO7	333	470	8.3	25*50	0.64 ⁽⁺⁾ 0.64 ⁽⁻⁾	0.4	25*50	1.28	0.26	1.12	0.0	520		
11	Chen (2005)	TDP1	348	464	21.3	20*33	0.52 ⁽⁺⁾ 0.26 ⁽⁻⁾	0.21	23*23	0.89	0.28	1.7	0.075	75±35	End-hook	Cyclic
12		TDP2	348	464	23.3	20*33	0.52 ⁽⁺⁾ 0.52 ⁽⁻⁾	0.21	23*23	0.89	0.28	1.7	0.075	75±35		
13	Hertanto (2006)	DD1	344	478	24.8	20*33	0.52 ⁽⁺⁾ 0.52 ⁽⁻⁾	0.21	23*23	0.89	0.28	1.7	0.075	75±35	End-hook	Biax-cyclic

Table 1 Continued

Specimen ID	Reference	Label	f_{ym} (MPa)	f_{tm} (MPa)	f_{cm} (MPa)	Beam section (cm*cm)	$\rho_{long,b}$ (%)	$\rho_{transv,b}$ (%)	Column section (cm*cm)	$\rho_{long,c}$ (%)	$\rho_{transv,c}$ (%)	L_b/L_c	$\rho_{transv,j}$ (%)	P (KN)	Long. reinf. details	Loading protocol
14	Liu (2001)	EJ2	321	-	29.2	30*50	1.0 ⁽⁺⁾ 0.66 ⁽⁻⁾	0.05	46*46	0.85	0.04	1.0	0.025	-	Bent	Cyclic
15		EJ4	321	-	36.5	30*50	1.0 ⁽⁺⁾ 0.66 ⁽⁻⁾	0.05	46*46	0.85	0.04	1.0	0.025	1700		
16	Beschi <i>et al.</i> (2012)	CJ1	365 445	558 546	38.7	30*50	0.42 ⁽⁺⁾ 0.28 ⁽⁻⁾	0.16	30*30	0.89	0.12	1.42	0.0	206	End-hook	Cyclic

Table 2 Properties of RC interior beam-column joint specimens considered in this study

Specimen ID	Reference	Label	f_{ym} (MPa)	f_{tm} (MPa)	f_{cm} (MPa)	Beam section (cm*cm)	$\rho_{long,b}$ (%)	$\rho_{transv,b}$ (%)	Column section (cm*cm)	$\rho_{long,c}$ (%)	$\rho_{transv,c}$ (%)	L_b/L_c	$\rho_{transv,j}$ (%)	P (KN)	Long. reinf. details	Loading type
1	Braga <i>et al.</i> (2009)	C23-1	350	460	14.5	20*33	0.49 ⁽⁺⁾ 0.32 ⁽⁻⁾	0.12	20*20	1.13	0.12	1.4	0.0	120	Continuous	Cyclic
2		C23-1	350	460	14.5	20*33	0.49 ⁽⁺⁾ 0.32 ⁽⁻⁾	0.12	20*20	1.13	0.12	1.4	0.0	120		
3		C11-1	350	460	14.5	30*50	0.49 ⁽⁺⁾ 0.32 ⁽⁻⁾	0.12	30*30	1.13	0.12	1.4	0.0	270		
4	Fernandes <i>et al.</i> (2013)	JPA-1	590	640	19.8	30*40	0.18 ⁽⁺⁾ 0.37 ⁽⁻⁾	0.17	30*30	0.5	0.13	1.35	0.0	200	Continuous	Cyclic
5		JPA-2	590	640	19.8	30*40	0.18 ⁽⁺⁾ 0.37 ⁽⁻⁾	0.17	30*30	0.5	0.13	1.35	0.0	200		
6		JPB	590	640	19.8	30*40	0.18 ⁽⁺⁾ 0.37 ⁽⁻⁾	0.17	30*30	1.0	0.13	1.35	0.0	450		
7		JPD	590	640	19.8	30*40	0.18 ⁽⁺⁾ 0.37 ⁽⁻⁾	0.34	30*30	1.0	0.34	1.35	0.0	450		

Table 2 Contined

Specimen ID	Reference	Label	f_{ym} (MPa)	f_{tm} (MPa)	f_{cm} (MPa)	Beam section (cm*cm)	$\rho_{long,b}$ (%)	$\rho_{transv,b}$ (%)	Column section (cm*cm)	$\rho_{long,c}$ (%)	$\rho_{transv,c}$ (%)	L_b/L_c	$\rho_{transv,j}$ (%)	P (KN)	Long. reinf. details	Loading type
8	Pampanin <i>et al.</i> (2003)	C2	345	458	23.9	20*33	0.49 ⁽⁺⁾ 0.32 ⁽⁻⁾	0.11	20*20	0.75	0.10	1.5	0.0	120	Continuous	Cyclic
9	Liu (2001)	Unit 1	321	-	44	30*50	1.3 ⁽⁺⁾ 0.68 ⁽⁻⁾	0.05	30*46	2.0	0.08	1.2	0.0	-	Continuous	Cyclic
10		Unit 2	321	-	49	30*50	1.3 ⁽⁺⁾ 0.68 ⁽⁻⁾	0.05	30*46	2.0	0.08	1.2	0.0	750		

Table 3 Properties of ductile RC column specimens considered in this study

Specimen ID	Reference	Label	Section (cm*cm)	ρ_{long} (%)	ρ_{transv} (%)	f_{ym} (MPa)	f_{tm} (MPa)	f_{cm} (MPa)	P (KN)	V (KN)	Long. reinf. detail	Loading protocol	
1	Verderame <i>et al.</i> (2008a)	M270a-1	30*30	0.75	0.33	355	470	25	270	40.8	Overlapped	Monotonic	
2		M270a-2	30*30	0.75	0.33	355	470	25	270	39.2			
3		M540a-1	30*30	0.75	0.33	355	470	25	270	62.6			
4		M270b-1	30*30	0.75	0.33	355	470	25	540	41.6			
5		M270b-2	30*30	0.75	0.33	355	470	25	540	42.4			Continuous
6		M540b-1	30*30	0.75	0.33	355	470	25	540	63.2			
7	Verderame <i>et al.</i> (2008b)	C270a-1	30*30	0.75	0.33	355	470	25	270	42.9	Overlapped	Cyclic	
8		C270a-2	30*30	0.75	0.33	355	470	25	270	43.0			
9		C540a-1	30*30	0.75	0.33	355	470	25	270	64.9			
10		C270b-1	30*30	0.75	0.33	355	470	25	540	39.9			
11		C540b-1	30*30	0.75	0.33	355	470	25	540	61.1			Continuous
12		C540b-2	30*30	0.75	0.33	355	470	25	540	64.6			
13	Marefat <i>et al.</i> (2008)	CCB9a	30*25	0.83	0.23	356	490	17.8	225	41.7	Continuous	Cyclic	

Table 3 Continued

Specimen ID	Reference	Label	Section (cm*cm)	ρ_{long} (%)	ρ_{transv} (%)	f_{ym} (MPa)	f_{tm} (MPa)	f_{cm} (MPa)	P (kN)	V (kN)	Long. reinf. detail	Loading protocol
14	Arani <i>et al.</i> (2013)	WOS-M	25*25	0.72	0.20	370	529	23.9	230	49.7	Continuous	Cyclic
15		WOS-C	25*25	0.72	0.20	370	529	22.9	230	57.1		
16		SOS-C	25*25	0.72	0.20	370	529	24.0	230	59.6	Overlapped	
17		HOS-C	25*25	0.72	0.20	370	529	24.8	230	59.2		
18	Diludovico <i>et al.</i> (2014)	S300P-c	30*30	1.0	0.22	330	445	18.9	340	54.1	Continuous	Cyclic
19		R300P-c	30*50	0.9	0.22	330	445	18.9	280	67.7		
20		R500P-c	50*30	0.9	0.14	330	445	18.9	280	119.5		
21	Diludovico <i>et al.</i> (2013)	S45P-1	30*30	1.0	0.22	330	445	21.1	380	44.5	Continuous	Biaxial cyclic
22		S30P-1	30*30	1.0	0.22	330	445	21.1	380	52.2		
23		S45P-2	30*30	1.0	0.22	330	445	21.1	380	42.3		
24		S30P-2	30*30	1.0	0.22	330	445	21.1	380	58.4		

Table 4 Properties of brittle RC column specimens considered in this study

Specimen ID	Reference	Label	Section (cm*cm)	ρ_{long} (%)	ρ_{transv} (%)	f_{ym} (MPa)	f_{tm} (MPa)	f_{cm} (MPa)	P (kN)	V (kN)	Transv. reinf. detail *	Loading protocol	Column type **
1	Henkhaus (2010)	# 1	≈ 45*45	1.50	0.07	455	655	19.98	1513	565	Type A	Cyclic	Short
2		# 2		1.50	0.07	455	655	19.29	1513	521		Cyclic	
3		# 3		1.50	0.07	455	655	22.05	979	561		Biaxial	
4		# 4		2.50	0.07	441	634	24.12	2225	716		Cyclic	
5		# 5		2.50	0.07	441	634	23.43	2225	699		Biaxial	
6	Henkhaus (2010)	# 6	≈ 45*45	2.50	0.18	489	710	27.56	668	334	Type B	Biaxial	Slender
7		# 7		2.50	0.18	489	710	28.25	668	334	Type A		
8		# 8		2.50	0.10	489	710	28.94	668	338			
9	Woods and Matamoros (2010)	S3	≈ 45*45	3.1	0.07	448	-	17.72	2225	312	Type A	Cyclic	Slender
10		S4		2.5	0.18	448	-	19.79	668	316	Type B		

Table 4 Continued

Specimen ID	Reference	Label	Section (cm*cm)	ρ_{long} (%)	ρ_{transv} (%)	f_{ym} (MPa)	f_{tm} (MPa)	f_{cm} (MPa)	P (kN)	V (kN)	Transv. reinf. detail *	Loading protocol	Column type **
11	Matchulat (2009)	S1	$\approx 45*45$	2.5	0.07	441	-	34.54	2225	414	Type A	Cyclic	Slender
12		S2		2.5	0.07	441	-	32.41	1513	360	Type B		
13	Sezen (2002)	2CHD12	$\approx 45*45$	2.5	0.18	441	-	21.10	2670	360	Type B	Cyclic	Slender
14		2CLD12		2.5	0.18	441	-	21.10	668	312			
15	Lynn (2001)	3CLH18	$\approx 45*45$	3.1	0.07	331	-	26.89	503	271	Type A	Cyclic	Slender
16		3CMH18		3.1	0.07	331	-	25.75	1513	338	Type A		
17		3CMD12		3.1	0.18	331	-	25.75	1513	356	Type B		
18		2CMH18		1.9	0.07	331	-	27.66	1513	316	Type A		

*Type A: 90-degree hooks; Type B: 90-degree hooks + diamond ties

**Short: $h_c/d_c < 3$; Slender: $h_c/d_c \geq 3$

Drift-based fragility functions provide information about the probability of experiencing (or exceeding) a particular damage state as a function of the peak interstory (or column) drift ratio experienced by the RC member. In other words, they provide the probability of experiencing or exceeding a particular damage state conditioned on the peak interstory (or column) drift.

Table 5 Interstory drift ratios used to develop fragility functions for exterior/interior beam-column joints

Component type	Specimen ID	IDR _{DS1} (%)	IDR _{DS2} (%)	IDR _{DS3} (%)	Component type	Specimen ID	IDR _{DS1} (%)	IDR _{DS2} (%)	IDR _{DS3} (%)	
External beam-column joints	1	0.85	1.25	1.75	Internal beam-column joints	1	0.875	2.25	3	
	2	-	0.9	2.2		2	0.75	1.75	2.75	
	3	0.65	1.1	1.5		3	0.75	2	3	
	4	0.4	1.53	3		4	0.83	2.3	3.3	
	5	0.6	2.39	4		5	0.64	1.8	3	
	6	0.6	1.72	3		6	0.46	1.5	2.3	
	7	0.7	1.61	4		7	0.48	1.6	3.3	
	8	0.4	1.42	3		8	0.6	2.1	3.1	
	9	0.6	2.23	4		9	-	1.8	2.8	
	10	0.4	1.51	3		10	-	2	2.1	
	11	0.8	1.33	2.5						
	12	0.6	1.75	2.25						
	13	0.75	1.25	1.375						
	14	1	1.75	2.5						
	15	-	1.3	2.25						
	16	0.6	1.1	2						

Table 6 Column drift ratios used to develop fragility functions for ductile/brittle weak columns

Component type	Specimen ID	CDR _{DS1} (%)	CDR _{DS2} (%)	CDR _{DS3} (%)	Component type	Specimen ID	CDR _{DS1} (%)	CDR _{DS2} (%)	CDR _{DS3} (%)
Ductile weak columns	1	0.77	2.45	3.07	Brittle weak columns	1	0.69	1.1	1.3
	2	0.72	1.84	4.19		2	0.60	0.86	2.3
	3	0.71	1.25	-		3	0.85	0.9	1.33
	4	0.95	2.69	-		4	0.7	0.7	1.8
	5	0.96	1.44	3.02		5	0.53	0.68	1.0
	6	0.89	1.1	2.69		6	1.3	1.8	2.2
	7	0.79	1.75	3.4		7	1.25	1.75	2.8
	8	0.77	1.97	3.7		8	1.1	1.3	2.0

Table 6 Continued

Component type	Specimen ID	CDR _{DS1} (%)	CDR _{DS2} (%)	CDR _{DS3} (%)	Component type	Specimen ID	CDR _{DS1} (%)	CDR _{DS2} (%)	CDR _{DS3} (%)
	9	0.89	2.05	3.45		9	0.75	1.05	1.1
	10	0.95	1.72	5.35		10	0.8	1.2	2.1
	11	0.99	2.1	3.5		11	0.77	1.08	1.6
	12	0.97	1.85	2.45		12	0.82	2.0	3.1
	13	1.17	1.88	3		13	0.88	0.96	3.0
	14	0.63	1.33	2.5		14	0.86	1.0	2.15
	15	1	2.2	3.12		15	0.9	1.6	2.05
	16	1.1	1.97	3.12		16	0.98	0.98	0.95
Ductile weak columns	17	0.8	1.97	4	Brittle weak columns	17	0.95	0.85	1.9
	18	-	2.2	-		18	1.0	2.4	-
	19	-	2.15	-					
	20	-	1.9	-					
	21	0.9	1.15	2					
	22	0.8	1.2	2					
	23	0.98	1.47	2.45					
	24	1.05	1.47	2.45					
	-	-	-	-					
	-	-	-	-					

Usually, fragility functions take the form of lognormal cumulative distribution functions, having a median value, θ , and logarithmic standard deviation, or dispersion, β . The mathematical form for such a fragility function is

$$F_i(DS > ds_i | d = IDR) = \Phi\left(\frac{\ln(d / \theta_i)}{\beta_i}\right) \tag{1}$$

where $F_i(DS > ds_i | d = IDR)$ is the conditional probability that the component will experience or exceed the i -th damage state as a function of the attained interstory drift, d ; Φ denotes the standard normal (Gaussian) cumulative distribution function; θ_i is the median value of the probability distribution of drift ratios (i.e., the value of demand at which there is a 50% probability that a component will reach or exceed that damage state) and β_i is the logarithmic standard deviation, which accounts for uncertainty in the value of demand at which a component reaches a given damage state. To establish θ_i and β_i for each component type and damage state, the procedure described below has been followed.

In the first step, cumulative frequency distributions of interstory drift ratios corresponding to

each damage state have been obtained by plotting ascending-ordered drift ratios at which each damage state was experimentally observed to occur against $(i-0.5)/n$, where “ i ” is the position of the drift ratio in the ordered list of drift ratios and “ n ” is the number of specimens in which the drift associated with that damage state was identified. These cumulative frequency distributions provide information about the portion of the data set corresponding to each damage state that does not exceed a particular value of drift and represent empirically derived cumulative distribution functions.

In the second step, the ordered data have been revised to eliminate possible outliers from the bulk of data (i.e., values of drift that result significantly above or below θ_i). Indeed, it is possible that one or more tests have reported spurious values of demand that reflect experimental errors or misinterpretation of experimental results rather than true value of drift at which the specimen attained a given DS. According to the Annex H of FEMA P-58, the Peirce’s criterion (Ross 2003) has been applied to test and eliminate doubtful observations of drift ratio.

In the next step, the Method of Maximum Likelihood has been used to fit cumulative probability functions to the final data sets, assuming that the data were lognormally distributed. According to this method, the median value of the demand at which a given damage state is likely to initiate, θ_i , can be computed with the following equation

$$\theta_i = \exp\left(\frac{1}{N} \sum_{j=1}^N \ln(d_j)\right) \quad (2)$$

where N is the total number of data, d_j is the drift ratio in the j -th test at which the damage state under consideration occur.

For experimental tests in which specimens were subjected to slowly increasing displacement demand and where the interstory drift ratio corresponding to the onset of a given damage state was actually recorded or properly documented by the investigators, d_j is the observed data.

For experimental tests where specimens were subjected to increments of displacement demand, and the damage state was observed in the first cycle of the next demand increment, d_j is the interstory drift ratio at the midpoint of the demand increment that caused the attainment of that damage state.

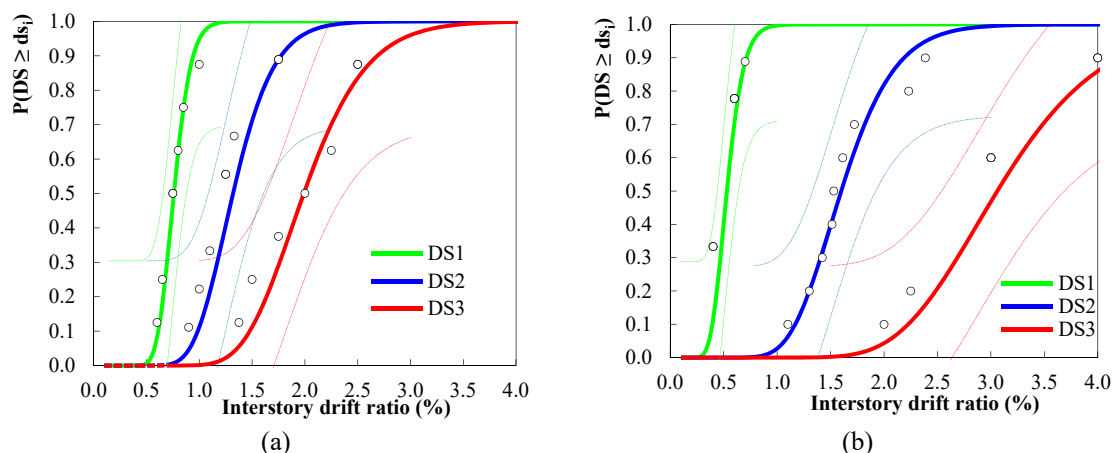


Fig. 6 Fragility functions fitted to interstory drift ratios corresponding to DS1, DS2, DS3 for external beam-column joints with (a) end-hook and (b) bent rebars

The value of the random dispersion, $\beta_{r,i}$ for the i -th DS, is given by

$$\beta_{r,i} = \sqrt{\frac{1}{N-1} \sum_{j=1}^N \left(\ln \left(\frac{d_j}{\theta_i} \right) \right)^2} \quad (3)$$

where N , d_j , and θ_i are as defined above. It is worth noting that the computed values θ and β_r are approximately, but not exactly, equal to the median and c.o.v. for each data set.

In the next step, Lilliefors goodness-of-fit testing (Lilliefors 1967) was carried out to verify the assumption of the lognormal distribution and evaluate the accuracy of the fragility parameters derived in the previous step. In accordance with Annex H of FEMA P-58, the fragility parameters have been deemed acceptable if the Lilliefors test passes, considering a 5% significance level.

In the last step, the computed distribution parameters have been adjusted to facilitate application in practice and account for uncertainty associated with the size of the data sets and differences between tests and actual building behavior, as discussed in detail in Section 5.5.

5.1 External beam-column joints

Fig. 6 shows the empirical cumulative distribution functions for three DSs of external beam-column joints with bars anchored in the joint with end-hooks (Fig. 6(a)) and bars bent in the joint (Fig. 6(b)), respectively. Also plotted in the graphs of Fig. 6 are the fitted lognormal cumulative distribution functions of interstory drift.

As can be seen, the lognormal distributions fit the data relatively well. In order to further verify if the cumulative distribution functions could be assumed as lognormally distributed, a Lilliefors goodness-of-fit test has been conducted. Also shown in Fig. 6 are graphical representations of this test for 5% significance levels. The hypothesis that the assumed cumulative probability distributions adequately fit the empirical data is accepted since all data points lie between the two thin lines.

The fragility function parameters for external RC beam-column joints are given in Table 7. The median values (θ) of interstory drift ratio have been rounded to the nearest 0.05% to facilitate use. As can be seen, the longitudinal reinforcement details play a not negligible role, determining greater values of θ (%) in presence of end-hooks at DS1 and in presence of bent bars at DS2 and DS3. On the contrary, the dispersion parameter (β_r) is almost the same (around 0.23-0.26), regardless reinforcement details and selected DS. Generally speaking, Fig. 6 points out that DS1 (light cracking) is not likely to be observed if the interstory drift is smaller than about 0.5% for end-hook bars and 0.25% for bent bars, and would be almost certain to occur if the peak interstory drift ratio is larger than 1.1% for end-hook bars and 0.9% for bent bars. Similarly, DS2 (severe cracking) would not be likely to be observed if the peak interstory drift is smaller than 0.7% for end-hook bars and 0.8% for bent bars, but it is almost certain to occur if the peak interstory drift ratio exceeds 2.2% for end-hook bars and 2.8% for bent bars. Finally, DS3 (spalling and crushing) would be not expected to occur for interstory drifts less than 1.0% for end-hook bars and 1.5% for bent bars, while it is almost certain to occur for interstory drifts greater than 3.5% for end-hook bars and 5.0% for bent bars.

In order to obtain an estimate of the probability of experiencing loss of vertical carrying capacity, for each specimen that was subjected to further cyclic loading after the development of the concrete wedge expulsion collapse mechanism, the following ratio was computed

$$\alpha = IDR_{DS4} / IDR_{DS3} \quad (4)$$

where IDR_{DS3} is the interstory drift ratio at which DS3 is deemed to occur and IDR_{DS4} is the interstory drift ratio at which the test was stopped. The α parameter provides a conservative estimate of the drift at which loss of vertical carrying capacity occurs. Based on the available data (relevant to nine specimens), α ranges from 1.17 to 2.55 with an average value of 1.68. In first approximation, the interstory drift ratio at which loss of vertical carrying capacity occurs in external beam-column joints can be assumed to be lognormally distributed (for brevity not shown in the paper) with median $IDR_{DS4} = 1.56 * IDR_{DS3}$ and logarithmic standard deviation equal to 0.264. The fragility function computed using these statistics provides a conservative estimate of the probability of losing vertical carrying capacity at a given drift.

5.2 Internal beam-column joints

Fig. 7 shows cumulative distribution functions for DS1, DS2 and DS3 of internal beam-column joints. Minor differences between IWBs and IWCs fragility groups are observed. For that reason,

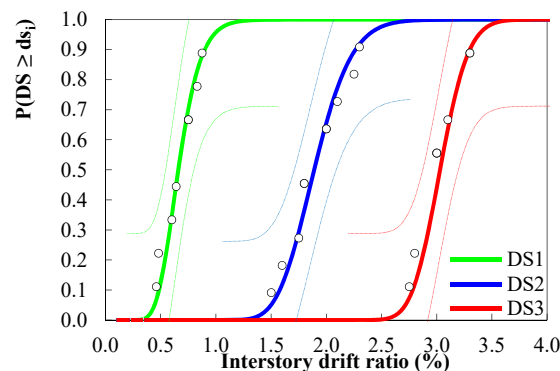


Fig. 7 Fragility functions fitted to interstory drift ratios corresponding to DS1, DS2, DS3 for internal beam-column joints

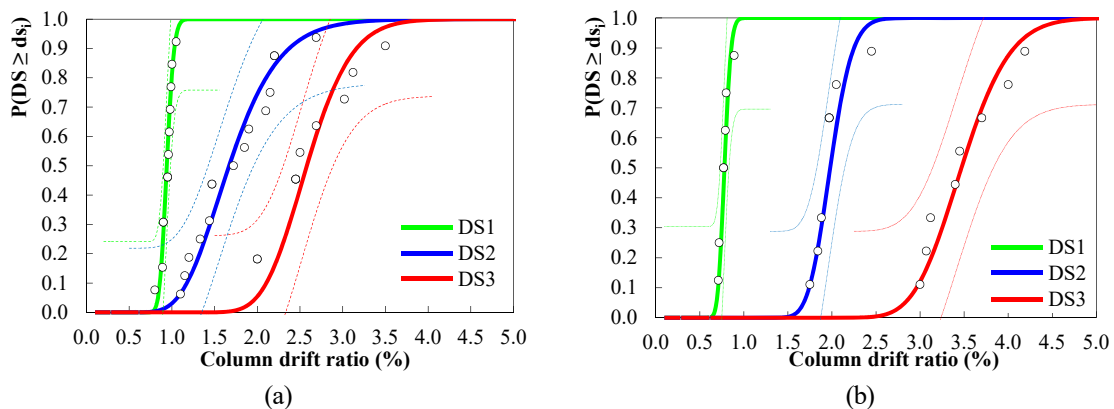


Fig. 8 Fragility functions fitted to column drift ratios corresponding to DS1, DS2, DS3 of ductile weak columns with (a) continuous and (b) lap-spliced rebars

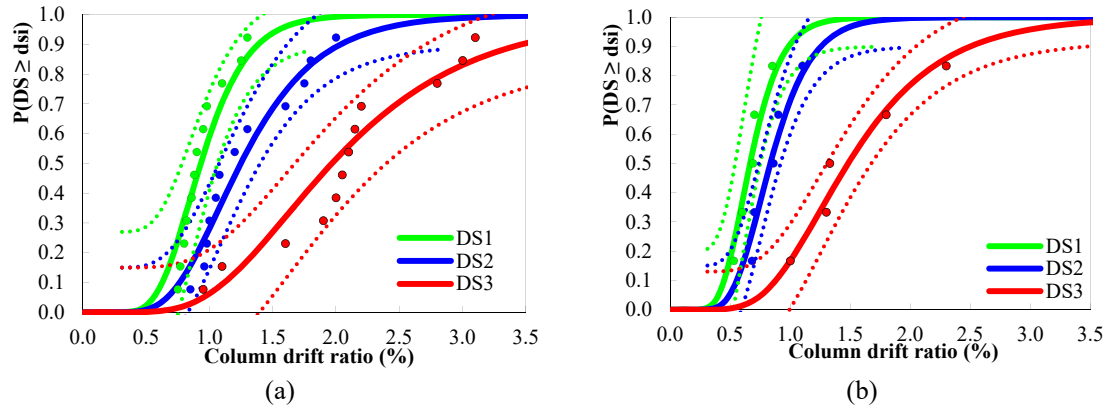


Fig. 9 Fragility functions fitted to column drift ratios corresponding to DS1, DS2, DS3 of (a) slender and (b) short brittle weak columns

the relevant interstory drift ratios are plotted together in Fig. 7. Also plotted in Fig. 7 are the fitted lognormal cumulative distributions and a graphical representation of the Lilliefors goodness-of-fit test for 5% significance levels that verifies the adequacy of the lognormal distribution assumption. The fragility function parameters for internal RC beam-column joints are given in Table 7.

5.3 Ductile weak columns

Fig. 8 shows the empirical cumulative distribution functions for the three DSs of ductile weak columns with continuous (Fig. 8(a)) and overlapped (Fig. 8(b)) bars, respectively. Also plotted in the figures are the fitted lognormal cumulative distribution functions together with a graphical representation of the Lilliefors goodness-of-fit test for 5% significance levels. The fragility function parameters, rounded to the nearest 0.05%, are listed in Table 7.

For DS1 negligible differences between columns with overlapped and continuous bars are found. In particular, DS1 (light cracking) would not be observed for drift ratios smaller than about 0.6-0.7%, while it would be almost certain to occur for drift ratios greater than 1.0-1.1%. DS2 (severe cracking) is not expected to occur for drift ratios smaller than 0.9% for continuous bars and 1.5% for overlapped bars, while it is almost certain to occur if the drift ratio exceeds 3% for continuous bars and 2.5% for overlapped bars. Similarly, DS3 (spalling and crushing) is unlikely to occur for drift ratios smaller than 1.7% for continuous bars and 2.5% for overlapped bars while it is almost certain to occur for drift ratios greater than 4% for continuous bars and 4.5% for overlapped bars.

5.4 Brittle weak columns

Fig. 9 shows the empirical cumulative distribution functions for (a) short and (b) slender brittle weak columns, respectively. Also plotted in the same figure are the fitted lognormal cumulative distribution functions and a graphical representation of the Lilliefors goodness-of-fit test for 5% significance levels. The fragility function parameters, rounded to the nearest 0.05%, are listed in Table 7.

For DS1 negligible differences between short and slender columns are observed. In particular,

Table 7 Proposed fragility parameters for performance-based seismic evaluation of pre-70 RC frame buildings

Structural component	Fragility groups	Damage states	Fragility function parameters			
			Median IDR/CDR (%)	Dispersion		
				β_r	β_u	β
External beam-column joints	Weak joints, beam flexural response ^{(a),(b)}	DS1: light cracking at beam/column-joint interfaces, yielding of beam rebars, possible first inclined crack in the joint	0.75% ^(a) 0.55% ^(b)	0.17 ^(a) 0.23 ^(b)	0.35	0.40
		DS2: severe beam and joint cracking, possible spalling of joint cover concrete	1.25% ^(a) 1.50% ^(b)	0.24 ^(a) 0.25 ^(b)	0.30	0.40
		DS3: spalling of joint cover concrete, possible crushing of concrete at beam-joint interface, possible buckling of rebars	2.00% ^(a) 2.75% ^(b)	0.25 ^(a) 0.26 ^(b)	0.30	0.40
		Internal beam-column joints	Weak beams (columns), with columns (beams) flexural response	DS1: light cracking at beam-joint interfaces DS2: extensive cracking, possible spalling of cover concrete DS3: concrete cover spalling on beams, possible crushing of concrete at beam-joint interface	0.65% 1.75% 3.00%	0.24 0.14 0.07
Columns	Ductile columns ^{(c),(d)}	DS1: yielding of column rebars, light opening of crack at the base of the column (fixed-end rotation mechanism)	0.75% ^(c) 0.90% ^(d)	0.07 ^(c) 0.07 ^(d)	0.35	0.40
		DS2: opening of large cracks due to fixed-end rotation at the base of the column, possible spalling of cover concrete	1.75% ^(c) 1.65% ^(d)	0.10 ^(c) 0.27 ^(d)	0.30 ^(c) 0.25 ^(d)	0.35
		DS3: loss of strength due to cover concrete spalling, possible concrete crushing, possible buckling of steel rebars	3.0% ^(c) 2.5% ^(d)	0.12 ^(c) 0.15 ^(d)	0.30	0.35
	Brittle columns ^{(e),(f)}	DS1: light cracking in the upper and lower thirds of the column	0.65% ^(e) 0.95% ^(f)	0.17 ^(e) 0.18 ^(f)	0.25	0.30
		DS2: extensive diagonal cracks along the entire height of the column	0.85% ^(e) 1.25% ^(f)	0.19 ^(e) 0.29 ^(f)	0.35 ^(e) 0.25 ^(f)	0.40
		DS3: Opening of large cracks. Buckling of steel rebars. Residual lateral strength. Possible significant loss of gravity load capacity.	1.5% ^(e) 2.0% ^(f)	0.28 ^(e) 0.33 ^(f)	0.25	0.40

(a) Beam bars anchored in the joint with end-hooks,

(b) Beam bars bent in the joint,

(c) Columns with overlapped longitudinal reinforcement,

(d) Columns with continuous longitudinal reinforcement.

(e) Short Columns,

(f) Slender Columns.

DS1 (light cracking) would not be observed for drift ratios smaller than about 0.3-0.4%, while it would be almost certain to occur for drift ratios greater than 1.25% for short columns and 1.5% for slender columns. DS2 (shear failure) is not expected to occur for drift ratios smaller than 0.4-0.5%, while it is almost certain to occur if the drift ratio exceeds 1.5% for short columns and 2.5% for

slender columns. Similarly, DS3 (loss of gravity load capacity) is unlikely to occur for drift ratios smaller than 0.6-0.7% while it is almost certain to occurs for drift ratios greater than 3.5% for short columns and 4.5% for slender columns.

5.5 Adjusting fragility functions to account for epistemic uncertainties

The dispersion β in Eq. (1) represents uncertainty in the actual value of interstory drift ratio at which a damage state is likely to occur. When fragility parameters are determined on the basis of a limited number of test data, two contributors to uncertainty must be considered. The first contribution, termed β_r , represents the random variability that is observed in the test data from which the fragility parameters have been derived (see Eq. (3)). It has been computed in the previous paragraphs, for each structural component, following the Method of Maximum Likelihood. The second contribution, termed β_u , takes into account uncertainty that the tests represent actual conditions of construction/installation and loading of components in a building, and uncertainty that the available data are an adequate sample size to accurately represent the true random variability. In this paragraph the values selected for β_u are discussed. The total dispersion, β , is then computed as

$$\beta = \sqrt{\beta_r^2 + \beta_u^2} \tag{5}$$

The dispersion parameter β_u has been assigned to account for uncertainty associated with actual building conditions and lack of data, following the recommendations provided in Appendix F of FEMA-P-58. As shown in Table 5, the values selected for β_u range from 0.25 to 0.35, with larger values assigned where data sets are smaller and to maintain consistent trends in dispersion across damage states and fragility groups. As a result, values of the total dispersion β ranging from 0.3 to 0.4 have been obtained. It should be noted that the total dispersion values have been rounded to the nearest 0.05 to facilitate use.

The fragility functions developed before can be used to estimate the probability that a given RC component is at a specific damage state when it is subjected to a certain level of interstory (or

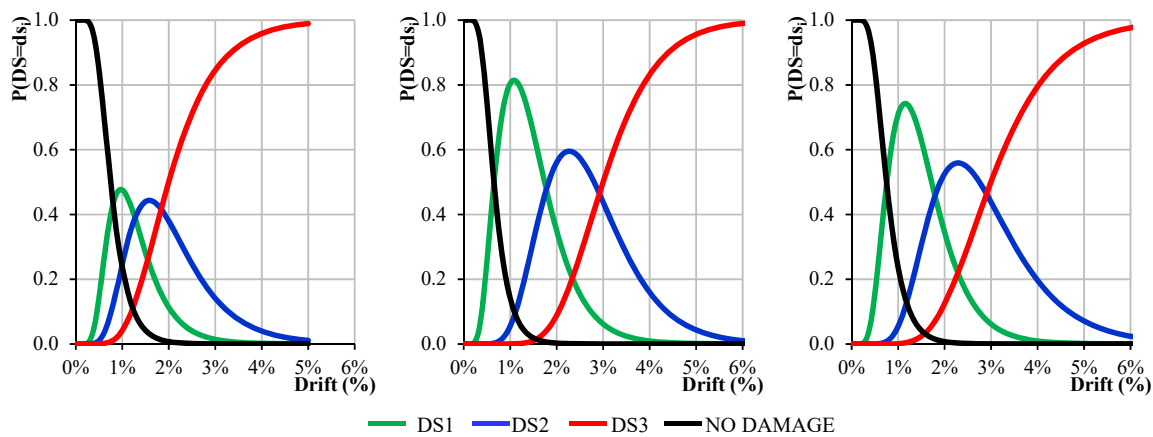


Fig. 10 Probability of being at each damage state for (a) EWJs, (b) IWBs and (c) DWCs

column) drift ratio. This probability can be estimated as the arithmetic difference between fragility functions corresponding to two consecutive damage states as follows

$$P(DS = ds_i, IDR_k) = \begin{cases} 1 - P(DS \geq ds_1 | IDR = IDR_k) \\ P(DS \geq ds_1 | IDR = IDR_k) - P(DS \geq ds_2 | IDR = IDR_k) \\ P(DS \geq ds_3 | IDR = IDR_k) \end{cases} \quad (6)$$

Fig. 10 shows the probability functions of being in each damage state for (a) EWJs, (b) IWBs and (c) DWCs, respectively. For instance, for external beam-column joints (see Fig. 10(a)), experiencing 1% peak interstorey drift, the probability of being in the first DS is 47.5%, 24.7% in the second DS and 4.2% in the third DS. However, there is also a 23.6% probability that the joint has not experienced any significant damage. At 3% drift, instead, the joint for sure has experienced significant damage and there is a 14.4% probability that it is in the second DS and 84.4% in the third DS.

6. Repair costs and loss functions

Economic losses associated with repair costs for damaged RC components can be expressed in terms of loss functions. Loss functions are defined as probabilistic estimates of the costs associated with the repair or replacement actions required in individual structural components when a specific damage state is reached. Loss function, therefore, provides information on the probability of experiencing a certain level of monetary loss when a given damage state is attained. In other words, they provide the probability of occurrence of a level of economic loss conditioned on the attainment of a given damage state in a component.

In this study, a set of normalized loss functions have been developed for each fragility group, in an attempt to extend the applicability of the results found in this study to as many situations as possible.

Considering structural repairing only, normalized loss functions can be expressed as follows

$$l_j | DS_i = \frac{RC_j | DS_i}{a_j} \quad (7)$$

where $l_j | DS_i$ is the economic loss in the j -th component conditioned on the occurrence of the i -th damage state, $RC_j | DS_i$ is the repair cost for the j -th component when the i -th damage state has occurred; a_j is the replacement cost of the j -th component, i.e., the construction cost required to rebuild the same component.

First of all, each damage state has been univocally associated with a specific set of repair activities that would be required to restore the structural component to its pre-earthquake (essentially undamaged) state. Most of the repair activities are common for all the FGs while differing passing from one DS to another, due to different extent and/or severity of damage. For ductile structural members, for instance, cracks can be repaired with epoxy injections, in order to restore the original strength and stiffness of the elements. Identifying the crack widths for which epoxy injection is an appropriate repair method is a critical issue. It seems suitable to use epoxy injections for crack

widths smaller than 5 mm (Pagni and Lowes 2006). Patching of concrete is adopted to replace spalled concrete. For wider crack widths (>5 mm) patching of concrete can be used instead of epoxy injections. Patching is accomplished removing loosened concrete and cleaning the adjacent surface. The critical issue is to identify the extent of spalled concrete for which patching is inadequate and a more effective repair method is required. Patching is considered to be inadequate if beam or column longitudinal reinforcement is exposed (Pagni and Lowes 2006), since patching would not be expected to restore concrete steel bond. In that case, removal and recast of damaged (and potentially damaged) concrete should be selected as repair method. In removing concrete, the objective is to ensure that only undamaged concrete remains as well as to ensure that a substantial volume of new material is placed around beam and/or column reinforcement to ensure that full bond capacity is recovered. Typically, the replacement material will be rheoplastic concrete mix, or special high-performance mortar mix. In some circumstances, it may be also necessary to replace a number of steel rebar(s), when either buckling or fracture occurs.

Generally speaking, repair activities are not limited to a series of specific repair actions for each RC member but they also include a number of preliminary and supplementary activities that can be summarized as follows:

- **Safety operations.** They include a number of preliminary operations carried out for safety reasons, such as: access protection, application of dust curtains, installation of scaffoldings and/or work platforms, installation of shoring adjacent to the columns to support gravity loads, etc..

- **Demolition activities.** This activity consists in the removal of furnishings and floor finishes, demolition of partition obstructing RC members to be repaired, isolation of mechanical, electrical and plumbing systems (as necessary) close to the intervention area. The extension of these preliminary works depends on the extension and severity of the structural damage, hence attained DS. For instance, the area of intervention for IWBs increases from 1.5 to 2.5 squared meters passing from DS1 to DS3.

- **Cleaning operations.** This activity consists in the removal of debris and clean of the area adjacent to main cracks and spalled/damaged concrete to be repaired. Obviously, the extension of these works depends on the extension and severity of the structural damage, hence attained DS. For example, the cleaning area for IWBs increases from half to total beam height passing from DS1 to DS3.

- **Replacement and Restoration.** This activity includes replacement of furnishings, restoration of partitions and floor finishes, replacement of mechanical, electrical and plumbing systems, as necessary.

- **Technical Costs.** Technical cost includes fees for structural engineer, project engineer, construction manager, etc. In first approximation, they have been assumed around 8% the total cost of the intervention.

Considering the total costs associated with structural repairing, normalized loss functions can be expressed as follows

$$L_j|DS_i = \frac{TC_j|DS_i}{b \cdot V_j} \quad (8)$$

where $L_j|DS_i$ is the total economic loss for the j-th component conditioned on the occurrence of the i-th damage state; $TC_j|DS_i$ is the total repair cost for the j-th component when the i-th damage state has occurred; b is the nominal cost per cubic meter of the building and V_j is the average volume surrounding the j-th component affected by the intervention. In first approximation, V_j has been taken equal to approximately 8 m³ for EWJs, 11 m³ for IWBs/IWCs and 6 m³ for DWCs/BWCs.

Table 8 summarizes the methods of repair considered for each DS of ductile RC members, together with a description of the related repair activities.

In the next step, the unit costs (c_k) for each repair action (see Table 9) have been estimated considering the Price List of Public Works in Basilicata Region, Italy (BUR 2013). Reference to the same document has been also made to estimate the additional costs related to the preliminary and complementary activities listed before. Within this context, further improvements and refinements could be achieved, for instance, by surveying designers and building firms to obtain a larger sample of repair methods and a more accurate database of repair costs.

In the next step, normalized repair cost ratios ($L_{C_j,DS_i}(50^{th})$) have been derived, based on quantity survey and cost estimate of a number of pre-70 RC frame buildings, including three archetype buildings, with number of storeys ranging from 4 to 8, and one 8-storeys real building, featuring perimeter frames and internal frames in one direction only.

$L_{C_j,DS_i}(50^{th})$ is defined as the average of the total repair cost (including all the preliminary and supplementary activities necessary to realize the intervention) for the j-th fragility group, due to the attainment of the i-th damage state, normalized by the nominal cost of the volume of the building affected by the intervention. From an analytic point of view, it can be expressed as follows

$$L_{C_j,DS_i}(50^{th}) = AVERAGE \left(\frac{(\alpha_1 + \alpha_2 + \alpha_3 + \alpha_4 + \alpha_5 + 1) \cdot \sum_k c_k u_k}{b \cdot V_j} \right) \quad (9)$$

where c_k is the unit cost for the k-th repair action, u_k is the associated quantity or extension of damage for the j-th fragility group, k is the total number of repair actions necessary for that

Table 8 Methods of repair and repair activities for ductile RC members

Damage State	Method of repair	Repair activities
DS1	Epoxy injection of concrete cracks	Install scaffolding and shoring systems. Remove furnishings, electrical and plumbing systems, as necessary. Demolish partitions, as necessary. Clean area adjacent to cracks. Prepare cracks. Inject cracks with epoxy resin. Restore finishes and partitions. Restore furnishings, electrical and plumbing systems as necessary. Remove scaffolding and shoring systems.
DS2	Patch concrete with mortar mix	Install scaffolding and shoring systems. Remove furnishings, electrical and plumbing systems, as necessary. Demolish partitions, as necessary. Remove loosened concrete and clean adjacent area. Inject cracks with epoxy resin. Patch concrete with mortar mix. Restore finishes and partitions. Restore furnishings, electrical and plumbing systems as necessary. Remove scaffolding and shoring systems.
DS3	Replace concrete (and rebars, if necessary)	Install scaffolding and shoring systems. Remove furnishings, electrical and plumbing systems, as necessary. Demolish partitions, as necessary. Remove damaged and potentially damaged concrete and clean adjacent area. Replace distorted rebars, if necessary. Inject cracks with epoxy resin. Replace concrete with rheoplastic concrete mix or high-performance mortar mix. Restore finishes and partitions. Restore furnishings, electrical and plumbing systems as necessary. Remove scaffolding and shoring systems.

Table 9 Unit costs for repair actions required for different damage states of RC members

Damage state	Repair Actions	Unit	Unit cost (€) (€/unit)
DS1 (Light cracking)	Clean area adjacent to cracks	m ²	6.61
	Prepare cracks to be injected	m ²	27.01
	Inject cracks with epoxy resin	m	156.00
DS2 (Severe cracking)	Remove loosened concrete, clean area adjacent to cracks	m ²	6.61
	Prepare cracks/surfaces to be injected /patched	m ²	27.01
	Inject cracks with epoxy resin	m	156.00
	Patch spalled concrete (if any) with mortar mix	m ²	88.35
	Steel jacketing *	m	216.87
DS3 (Spalling, crushing of concrete, buckling of rebars)	Remove damaged and potentially damaged concrete and clean adjacent area	m ²	6.61
	Prepare concrete surface to ensure full bond between new and existing concrete	m ²	27.01
	Inject cracks with epoxy resin	m	156.00
	Replace distorted bars (if any)	each	50
	Replace damaged concrete with rheoplastic concrete mix or high-performance mortar mix	m ²	109.26
	Demolition and re-construction *	m ³	668

*Only for Brittle Weak Columns (BWCs)

damage state; α_1 , α_2 , α_3 , α_4 and α_5 are magnification factors of the repair cost to account for all the preliminary and complementary activities involved in the intervention (see Fig. 11); b is the nominal cost per cubic meter of the building and V_j is an estimate of the volume of the building, surrounding the RC component, affected by the intervention.

To derive the nominal cost per cubic meter of the building (b) the following procedure has been followed. First, the replacement cost of the selected buildings has been estimated, assuming an average unit cost of 730 euro/m² for each floor of the building (Bassi 2014) less 90 euro/m² for shallow foundation. An additional cost of 44 euro/m³ has been then considered to account for demolition and waste disposal (CIAM 2014). The building cost per cubic meter (b) has been computed dividing the replacement cost of each building by its volume.

The repair cost ratio for each fragility group and damage state, has been disaggregated in different cost items (i.e., repair, safety, demolition, etc.). This way, the contribution of each repair activity to the total repair cost can be evaluated. The breakdown of the total repair cost for EWJs, IWBs and DWCs is shown in Fig. 11, for each DS. As expected, repair costs increase while increasing the severity and extension of damage (i.e., passing from DS1 to DS3), however, they do not exceed 15% of the total costs for repair at DS1 and 30% at DS3. The most important cost items are related to replace/restore activities and safety operations, which together represent approximately 50% of the total repair cost, regardless of the DS considered.

Eq. (9) provides reasonable estimates of the expected values of total repair costs (i.e., the 50th percentile levels), which are appropriate for estimating economic losses for many pre-70 RC frame buildings (see third column of Table 10). Eq. (9), however, does not provide information on how large economic losses can become in a given scenario. In other words, Eq. (9) does not provide

information on the dispersion around the average value.

Repair costs, indeed, are random variables. Based on the recommendations of FEMA P-58, it can be assumed that repair costs follow a cumulative lognormal distribution. Unfortunately, poor information are available on the statistics of specific repair actions at the component level, as well as on the correlation coefficients between different repair actions corresponding to different damage states in individual components. As a consequence, in this study, the simplified approach described below has been followed to derive loss functions for typical structural components of pre-70 RC frame buildings.

First, 10th and 90th percentile levels of the total repair costs have been estimated, from the 50th percentile values obtained before, based on engineering judgment. More precisely, two additional damage patterns, differing from the reference pattern, used to derive the best estimate (50th percentile) of the repair cost ratio, in the extent and severity of damage (e.g., more/less cracks to be injected, more/less cover concrete to be patched, etc.), have examined to estimate lower (say 10th) and higher (say 90th) percentile values of repair cost.

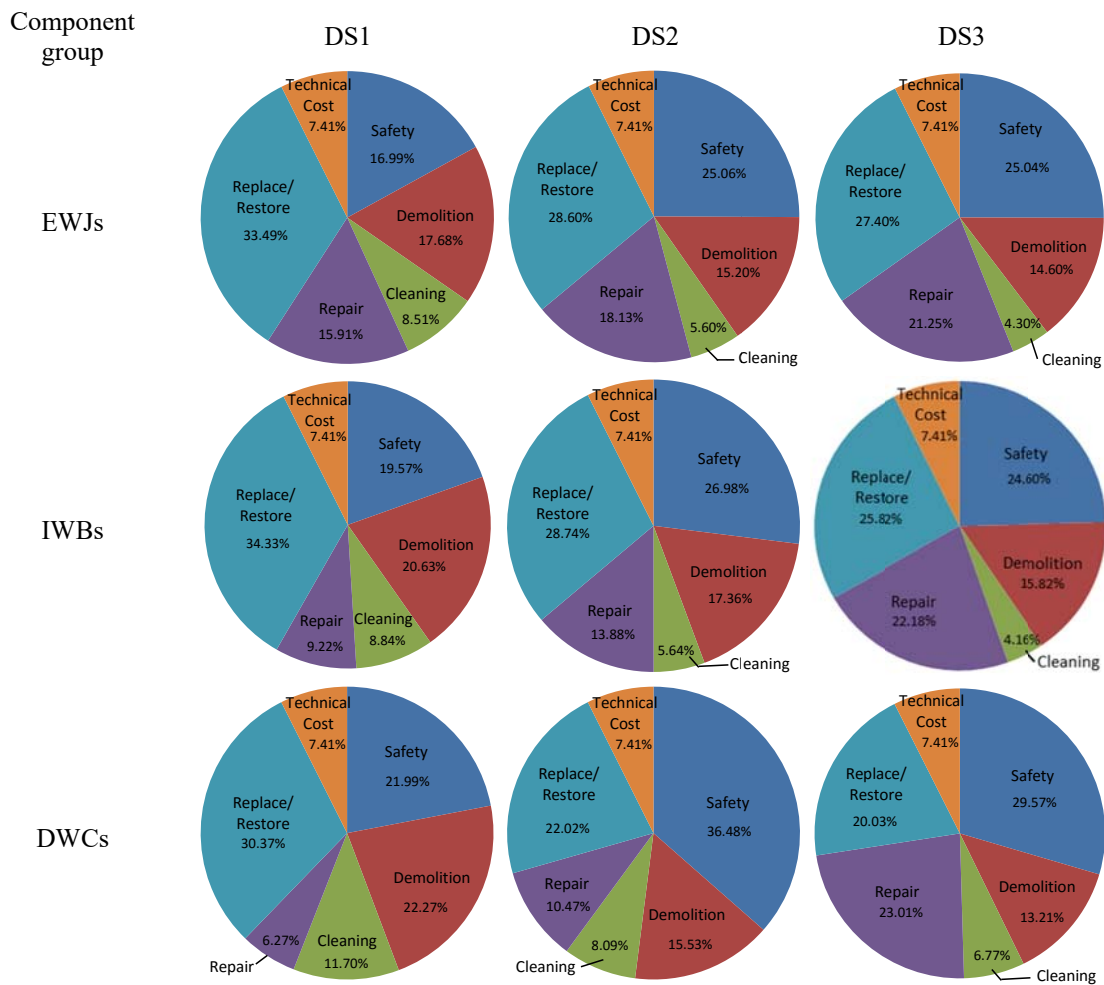


Fig. 11 Disaggregation of total repair costs for (a) EWJs, (b) IWBs and (c) DWCs, respectively

Cumulative lognormal distributions of the total repair cost ratios ($L_{C_j|DS_i}$) have been then derived by fitting the 10th, 50th, and 90th percentile estimates obtained in the previous step (see Fig. 12). The resultant median λ_{C_j,DS_i} and dispersion β_{C_j,DS_i} are reported in Table 10, for each fragility group and associated DS. As can be seen in Table 10, as the damage state level increases, the total repair cost ratio tends quickly to one meaning that for that type of RC components the repair costs are relatively high even for low levels of damage.

Finally, loss functions to be implemented in PACT have been drawn assuming, in line with the recommendation of FEMA P-58, a lower/upper quantity of components (q_{min}/q_{max}) below/above which there is no discount reflecting economies of scale or efficiencies in operation. Values of q_{min}/q_{max} and the associated maximum/minimum normalized total repair costs $\lambda_{max}/\lambda_{min}$ are reported in Table 10.

The normalized expected loss for the j-th fragility group ($E(L_{C_j}, IDR_k)$) can be computed as the sum of the products between the median value of the distribution of repair cost ratios associated with each DS (λ_{C_j,DS_i} in Table 10) and the probability of being in each DS (see Fig. 10)

$$E(L_{C_j}, IDR_k) = \sum_{i=1}^m \lambda_{C_j,DS_i} \cdot P(DS = ds_i, IDR_k) \tag{11}$$

where $m=3$ is the number of damage states for the j-th fragility group, $P(DS=ds_i, IDR_k)$ is the probability of the component being in the i-th damage state, when it is subjected to an interstory (or column) drift ratio IDR_k (CDR_k). Fig. 13 shows the expected loss for the main fragility groups considered in this study, as a function of the peak interstory (or column) drift ratio attained during an earthquake.

Table 10 (i) 50th percentile values of repair cost ratio $L_{C_j,DS_i}(50^{th})$, (ii) fitted median λ_{C_j,DS_i} and dispersion β_{C_j,DS_i} relevant to lognormal distributions of total repair cost ratios, and (iii) parameters to be implemented in PACT to describe loss functions of pre-70 RC frame buildings

Fragility Groups	Damage State	$L_{C_j,DS_i}(50^{th})$	λ_{C_j,DS_i}	β_{C_j,DS_i}	λ_{max}	λ_{min}	q_{max}	q_{min}
EWJs	DS1	0.71	0.74	0.45	0.96	0.59	20	5
	DS2	1.12	1.16	0.40	1.39	0.99	20	5
	DS3	1.51	1.57	0.42	1.88	1.33	20	5
IWBs	DS1	0.60	0.62	0.46	0.81	0.50	20	5
	DS2	0.98	1.02	0.41	1.22	0.86	20	5
	DS3	1.53	1.59	0.42	1.91	1.35	20	5
IWCs	DS1	0.67	0.70	0.46	0.81	0.50	20	5
	DS2	0.97	1.00	0.38	1.22	0.86	20	5
	DS3	1.27	1.32	0.42	1.91	1.35	20	5
DWCs	DS1	0.65	0.67	0.47	0.88	0.54	20	5
	DS2	0.97	0.99	0.37	1.19	0.85	20	5
	DS3	1.21	1.25	0.41	1.50	1.07	20	5
BWCs	DS1	0.54	0.54	0.30	0.70	0.43	5	3
	DS2	1.05	1.06	0.34	1.27	0.90	5	3
	DS3	10.67	10.92	0.29	13.11	9.28	5	3

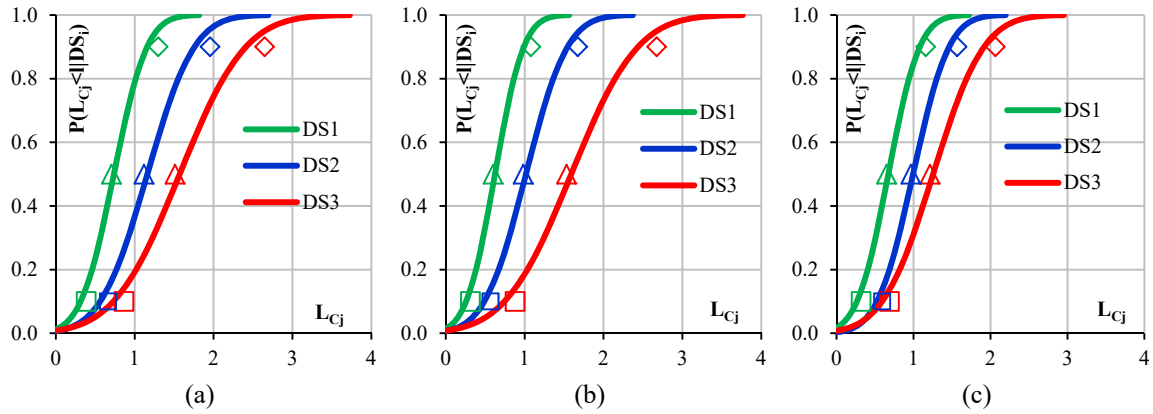


Fig. 12 Cumulative lognormal distributions of the total cost ratios for (a) EWJs, (b) IWBs and (c) DWCs

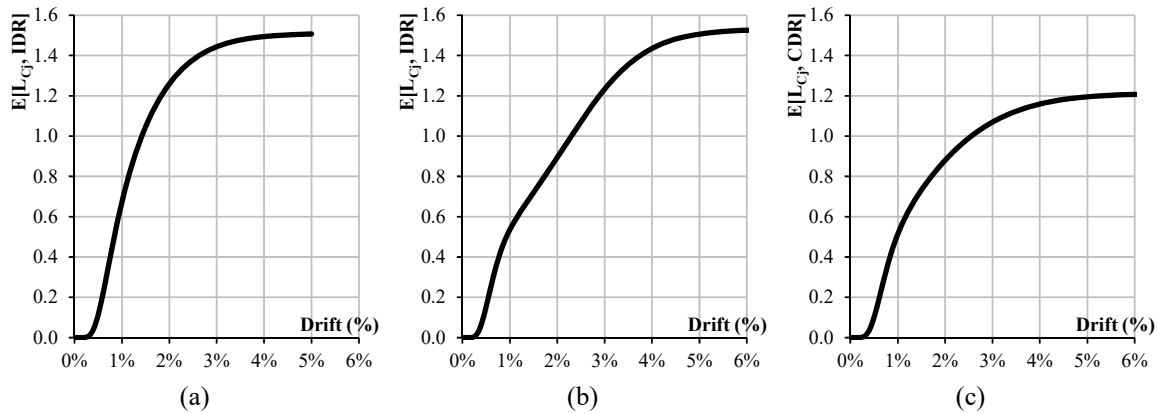


Fig. 13 Expected loss for (a) EWJs, (b) IWBs and (c) DWCs, respectively, for different levels of drift ratio

7. Conclusions

Fragility functions for the main structural components of pre-70 RC frame buildings have been derived, based on results of previous experimental studies. The attention has been focused on external/internal beam-column joints and ductile/brittle weak columns, designed for gravity loads only, using low-strength concrete and plain steel reinforcing bars. Repair costs for damaged RC structural components have been then estimated based on detailed quantity survey and cost estimate of a number of pre-70 RC buildings, using suitable costing manuals. Finally, loss functions that provide economic losses for individual RC components, as a function of the experienced peak interstory (or column) drift ratios, have been derived.

The fragility curves and loss function derived in this study have been implemented in the Performance Assessment Calculation Tool (PACT) of FEMA-P-58 for the loss assessment of older RC frame buildings (Cardone and Perrone 2016).

Acknowledgements

This work has been carried out within the Line 7 of the ReLUIIS/DPC 2014-2018 research program, dealing with direct displacement approaches for the evaluation of seismic losses of buildings in pre- and post- rehabilitation conditions. The author gratefully acknowledges the support of the RELUIIS Consortium for this research. The author is also grateful to Dr. G. Perrone for his valuable assistance in evaluating repair costs and bill of quantities.

References

- ACI - Committee 318 (1971), *ACI 318-71: Building Code Requirements for Reinforced Concrete*, American Concrete Inst., Farmington Hills, MI.
- Arani, K.K., Marefat, M.S., Amrollahi-Biucky, A. and Khanmohammadi, M. (2013), "Experimental seismic evaluation of old concrete columns reinforced by plain bars", *Struct. Des. Tall Spec. Build.*, **22**(3), 267-290.
- Aslani, H. and Miranda, E. (2005), "Probabilistic earthquake loss estimation and loss disaggregation in buildings", Report No. 157. Stanford, CA: John A. Blume Earthquake Engineering Center, Stanford University.
- ATC (2012), Applied Technology Council, *FEMA P-58 Next-generation Seismic Performance Assessment for Buildings, Vol. 1- Methodology*, Federal Emergency Management Agency, Washington, DC.
- ATC (2012), Applied Technology Council, *FEMA P-58 Next-generation Seismic Performance Assessment for Buildings, Vol. 2 - Implementation Guide*, Federal Emergency Management Agency, Washington, DC.
- Bassi, A. (2014), *Costi per tipologie edilizie. La valutazione economica dei progetti in fase preliminare*, Ed. Maggioli, Santarcangelo di Romagna (RN), Italy. (in Italian)
- Bedirhanoglu, I., Ilki, A., Pujol, S. and Kumbasar, N. (2010), "Behavior of deficient joints with plain bars and low-strength concrete", *ACI Struct. J.*, **107**(3), 300-310.
- Beschi, C., Riva, P. and Meda, A. (2012), "Corner beam-column joints retrofitting with HPFRC jacketing", *3rd International Conference on Concrete Repair, Rehabilitation and Retrofitting*, Cape Town, South Africa.
- Bozorgnia, Y. and Bertero, V.V. (2004), *Earthquake Engineering: From Engineering Seismology to Performance-Based Earthquake Engineering*, CRC Press.
- Bracci, J.M., Reinhorn, A.M. and Mander, J.B. (1995), "Seismic resistance of reinforced concrete frame structures designed for gravity loads: performance of structural system", *ACI Struct. J.*, **92**(5), 597-609.
- Braga, F., Gigliotti, R. and Laterza, M. (2009), "Existing RC structures with smooth bars: Experimental behavior of beam-column joints subject to cyclic lateral loads", *Open Construct. Build. Technol. J.*, **3**(1), 52-67.
- BUR (2013), *Price List of Public Works in Basilicata Region*, Official Journal of Regione Basilicata, Potenza. (in Italian)
- Calvi, G.M., Magenes, G. and Pampanin, S. (2002), "Relevance of beam-column joint damage and collapse in Rc frame assessment", *J. Earthq. Eng.*, **6**(S1), 75-100.
- Cardone, D. and Perrone, G. (2015), "Developing fragility curves and loss functions for masonry infill walls", *Earthq. Struct.*, **9**(1), 257-279.
- Cardone, D. and Perrone, G. (2016), "Damage and loss assessment of Pre-70 RC frame buildings with FEMA P-58", *J. Earthq. Eng.*, doi: 10.1080/13632469.2016.1149893.
- Chen, T.H. (2006), "Retrofit strategy of non-seismically designed frame systems", Master thesis, University of Canterbury, Christchurch, New Zealand.
- CIAM (2014), *Prezzi tipologie edilizie*, Ed., DEI, Collegio degli Ingegneri e degli Architetti di Milano, Roma, Italy. (in Italian)
- Di Ludovico, M., Verderame, G., Prota, A., Manfredi, G. and Cosenza, E. (2013), "Experimental behavior of non-conforming RC columns with plain bars under constant axial load and biaxial bending", *J. Struct. Eng.*, **139**(6), 897-914.
- Di Ludovico, M., Verderame, G.M., Prota, A., Manfredi, G. and Cosenza, E. (2014), "Cyclic behavior of non

- conforming full-scale RC columns”, *J. Struct. Eng.*, **140**(5), 897-914.
- El-Attar, A.G., White, R.N. and Gergely, P. (1997), “Behaviour of gravity load designed reinforced concrete buildings subjected to earthquakes”, *ACI Struct. J.*, **94**(2), 133-145.
- Fernandes, C., Melo, J., Varum, H. and Costa, A. (2013), “Cyclic behaviour of substandard reinforced concrete beam-column joints with plain bars”, *ACI Struct. J.*, **110**(1), 137-147.
- GU - Gazzetta Ufficiale (1974), *Provvedimenti per le costruzioni con particolari prescrizioni per le zone sismiche*, Legge 2 febbraio 1974, n. 64, published on GU n. 076 on 21/03/1974. (in Italian)
- Hakuto, S., Park, R. and Tanaka, H. (2000), “Seismic load tests on interior and exterior beam-column joints with substandard reinforcing details”, *ACI Struct. J.*, **97**(1), 11-25.
- Henkhaus, E. (2010), “Axial failure of vulnerable reinforced concrete columns damaged by shear reversals”, Ph.D. thesis, Purdue University, West Lafayette Indiana.
- Hertanto, E. (2005), “Seismic assessment of pre-1970s reinforced concrete structures”, Ph.D. thesis, New Zealand: University of Canterbury.
- ICBO - International Conference of Building Officials (1967), *Uniform Building Code*, Vol. 1, Whittier, CA.
- Lilliefors, H. (1967), “On the Kolmogorov-Smirnov test for normality with mean and variance unknown”, *J. Am. Statistic. Assoc.*, **62**(318), 399-402.
- Liu, A. and Park, R. (2001), “Seismic behaviour and retrofit of pre-1970’s as-built exterior beam-column joints reinforced by plain round bars”, *Bull. NZ. Soc. Earthq. Eng.*, **34**(1), 68-81.
- Lynn, A. (2001), “Seismic evaluation of existing reinforced concrete building columns”, Ph.D. thesis, University of California, Berkeley, California.
- Marefaf, M.S., Karbasi, K., Arani, S., Hassanzadeh, M.S. and Amrollahi, A. (2008), “Seismic behavior and retrofit of concrete columns of old R.C. buildings reinforced with plain bars”, *Seismic Engineering Conference commemorating the 1908 Messina and Reggio Calabria Earthquake*.
- Matchulat, L. (2009), “Mitigation of collapse risk in vulnerable concrete buildings”, MSc. thesis, University of Kansas, Lawrence.
- Pagni, C.A. and Lowes, L.N. (2006), “Fragility functions for older reinforced concrete beam-column joints”, *Earthq. Spectra*, **22**(1), 215-238.
- Pampanin, S., Calvi, G.M. and Moratti, M. (2002), “Seismic behavior of R.C. beam-column joints designed for gravity loads”, *Proceeding of 12th European Conference on Earthquake Engineering*, London, UK.
- Pan, A.D. and Moehle, J.P. (1988), “Reinforced concrete flat plates under lateral loading: an experimental study including biaxial effects”, Report UCB/EERC-88/16, University of California, Berkeley, CA.
- Ross, S.M. (2003), “Peirce’s criterion for the elimination of suspect experimental data”, *J. Eng. Technol.*, **20**(2), 38-41.
- Verderame, G.M., Fabbrocino, G. and Manfredi, G. (2008a), “Seismic response of RC columns with smooth reinforcement, part I: monotonic tests”, *Eng. Struct.*, **30**(9), 2277-2288.
- Verderame, G.M., Fabbrocino, G. and Manfredi, G. (2008b), “Seismic response of RC columns with smooth reinforcement, part II: Cyclic tests”, *Eng. Struct.*, **30**(9), 2289-2300.
- Woods, C. and Matamoros, A.B. (2010), “Effect of longitudinal reinforcement ratio on the failure mechanism of R/C columns most vulnerable to collapse”, *Ninth US National Conference and Tenth Canadian Conference on Earthquake Engineering*, Toronto, Canada.